Finite element analysis of effect of electrode pitting in resistance spot welding of aluminium alloy

B. H. Chang*[1], Y. Zhou[2], I. Lum[2] and D. Du[1]

The effect of electrode pitting on the formation of the weld nugget in resistance spot welding of an aluminium alloy was investigated using the finite element method. Pitted electrodes were simulated by assuming a pre-drilled hole of varying diameter at the centre of the electrode tip surface. The results showed that a small pitting hole would not have a detrimental influence on the nugget size. The actual contact area at the electrode/sheet interface did not change significantly when the diameter of the pitting hole was increased. However, a large pitted area at the electrode tip surface resulted in a greatly increased contact area and hence reduced current density at the sheet/sheet interface, which in turn led to the formation of an undersized weld nugget. The numerical calculation of the nugget shape and dimensions agreed well with experimental observations.

Introduction

Aluminium alloys are being increasingly used in the automobile industry owing to their light weight, and resistance spot welding (RSW) technology represents one of the most attractive methods for joining aluminium sheet bodies.[1] However, because of the relatively low electrical resistivity of aluminium alloys, the welding current necessary in RSW is much higher compared with that for steels. This, coupled with thick oxide films on the aluminium surface, will result in relatively high temperature at the electrode tip, and hence accelerated electrode degradation and reduced electrode life in RSW. For example, it has been found that the electrode life is only a few hundred spot welds in RSW of aluminium alloys,[2,3] compared with a few thousand spot welds when welding zinc coated steels.[4] Much of the prior work performed on electrode tip life during RSW of aluminium alloys has focused on the influences of polarity effects,[3] surface conditions of sheet and electrode,[5–7] and electrode design including copper alloys,[8] coating,[9] and configuration.[10] Chuko and Gould[11] have investigated the weld microstructure changes as electrodes wear, and correlated underlying weld microstructures with the various measures of electrode tip life performance. At present, detailed work on the mechanisms of electrode degradation during RSW of aluminium alloys remains very limited.[12–14]

It is generally thought that electrodes fail as a result of electrode pitting due to metallurgical interactions between the copper electrode and aluminium sheet.[12–14] Nevertheless, the influence of electrode pitting on the welding quality is uncertain at present. Some researchers think that the pitted electrode tip surface cannot provide a uniform contact and electric current flow path at the electrode/sheet interface, and therefore results in unsatisfactory weld spots and electrode failure;[12] another experimental investigation shows that the severely pitted electrode will cause a large increase in the contact area at the sheet/sheet interface, which is thought to lead to a reduction in current density and hence the formation of undersized weld nuggets.[13] Currently, no quantitative study has been carried out to address the issues of the nature and strength of the influence of pitting on the current density and temperature distributions at the contact interfaces, and to correlate the amount of pitting with the nugget dimensions formed in RSW. In the present work, finite element analysis is employed to study quantitatively the effect of electrode pitting on the weld nugget formation in RSW of aluminium alloy 5182, and the calculation results are compared with those of an experimental investigation.

## Experimental simulation and finite element modelling

Experimental simulation

In previous studies,[3] electrode tip life tests were performed to investigate electrode degradation in RSW of 1·5 mm thickness sheet aluminium alloy 5182 using a medium frequency direct current welder and Cu–0·15 wt-%Zr electrodes with a tip face diameter of

[1]Department of Mechanical Engineering, Tsinghua University, Haidian District, Beijing, 100084, People's Republic of China
[2]Department of Mechanical Engineering, University of Waterloo, 200 University Avenue West, Waterloo, Ont., N2L 3G1, Canada

*Corresponding author, email bhchang@mail.tsinghua.edu.cn
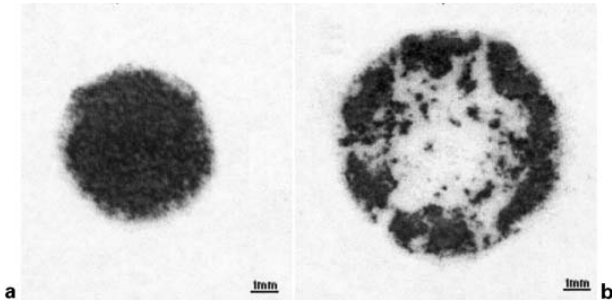
1 **Carbon paper imprints of electrode tip surfaces *a* at start of electrode life (0 welds) and *b* at end of electrode life (360 welds)**

10 mm and radius of curvature of 50 mm. The experimental results indicated that electrode degradation, as a result of metallurgical interactions between the copper electrode and aluminium sheet, occurred in four steps: aluminium pickup, electrode alloying with aluminium, electrode tip face pitting, and cavitation. A severely pitted electrode would result in electrode failure due to the formation of an undersize weld nugget.

Figure 1 shows the carbon paper imprints of the tip surfaces of a new and used electrode at the beginning and end of the electrode life, respectively. Perfect contact between electrode and sheet was achieved when the electrode was new. The severely pitted electrode at the end of its life exhibited a non-contacting region at the centre and an increased nominal contact diameter; this was because most of the central part was pitted and could no longer be brought into contact with the sheet surface during welding. To study further the effect of electrode pitting and cavitation on nugget formation, simulated electrodes (i.e. normal electrodes with a pre-drilled central hole of varying diameter from 1·0 to 5·0 mm to model the severity of electrode pitting, as shown in Fig. 2) were used in welding experiments. The same welding parameters as used in the electrode tip life tests were used, i.e. welding current of 29 kA, electrode force of 5 kN, squeeze time of 25 cycles, weld time of 5 cycles, and hold time of 12 cycles. It was observed that the outside diameter of the carbon imprints increased as the hole diameter varied (Fig. 3). Comparing Fig. 3 with Fig. 1, it could be seen that the varying degrees of pitting could be represented fairly well by simply increasing the centre cavity diameter. In the present experimental work, the diameters of the buttons from peeled samples were measured, and the cross-sections of
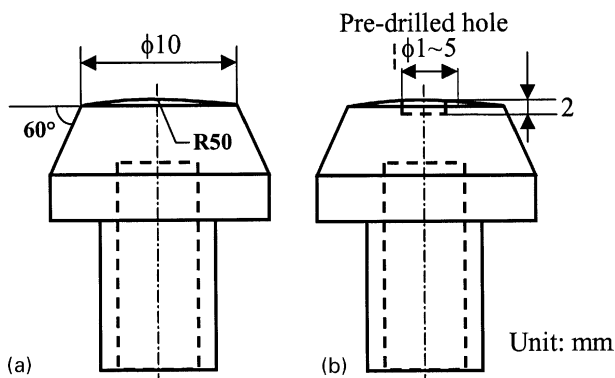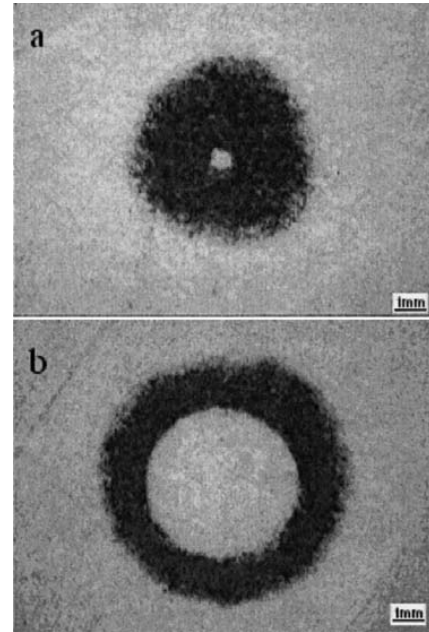
3 **Carbon paper imprints of electrodes with pre-drilled hole diameters of *a* 1·0 and *b* 5·0 mm**
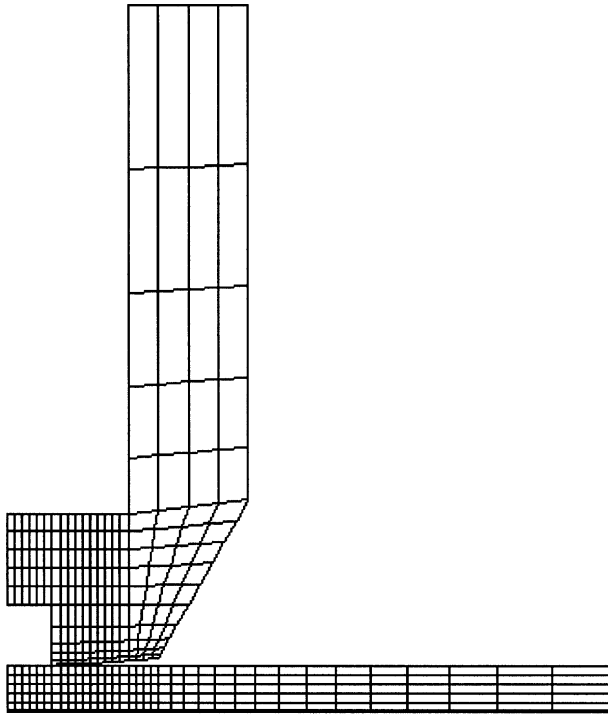
the nuggets formed were observed using an optical microscope.

Finite element modelling

The Ansys/MP5·7 (Ansys, Canonsburg, PA, USA) commercial finite element analysis code was employed in the present numerical analysis. The incrementally coupled electrical–thermal–mechanical algorithm developed in previous work[15] was adopted to model the RSW process using electrodes with pre-drilled holes of different diameters, and the fundamentally based contact resistance model derived from microcontact theory was included in the finite element analysis procedure to take the contact resistances at the electrode/sheet and sheet/sheet interfaces into account: details on how this contact resistance model was established and adopted in modelling can be found in Ref. 15.

As an example, the top half of the finite element mesh used for a hole diameter of 3·0 mm is shown in Fig. 4. The boundary conditions in electrical–thermal analysis were as follows:

(i) the voltage at the bottom end of the lower electrode was set to zero, and a direct current of 29 kA was applied at the top end of the upper electrode

(ii) the electric current flow and heat transfer across the electrode/sheet and sheet/sheet interfaces were only allowed for the parts in contact with each other – whether the nodes at the interfaces were in contact or not was determined from the node to surface contact elements in thermal–mechanical analysis of a time step; in the electrical–thermal analysis of the following time step, the parts in contact were coupled to allow the current to flow through, whereas parts not in contact were not coupled and therefore no current could flow through

(iii) studies by Browne *et al.*[16] showed that the convective heat transfer to the surrounding air is negligible and can be ignored, therefore the

2 **Dimensions of *a* normal and *b* pitting simulation electrodes**

4 Top half of finite element mesh when pitting hole diameter is 3·0 mm

5 Contact areas at electrode/sheet (E/S) and sheet/sheet (S/S) interfaces for electrodes with various diameters of pre-drilled hole under electrode force of 5·0 kN

outer surfaces for both electrode and sheets were assumed to be adiabatic – the effect of the cooling water in the electrode cavity was taken into account by assigning the ambient temperature (20°C) to the inner surfaces of the electrode. The boundary conditions used in the thermal–mechanical analysis included:
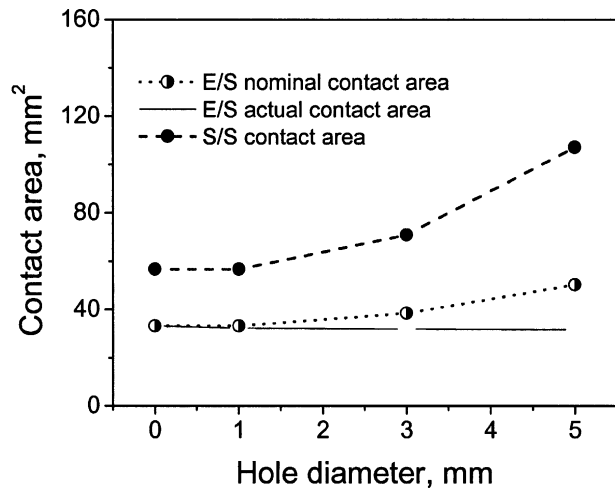
(i) electrode force was applied as a uniformly distributed pressure at the top end of the upper electrode; the temperature calculated from electrical–thermal analysis was applied as a body load

(ii) axial displacements at the bottom end of the lower electrode and radial displacement at the centreline were all constrained.

Aluminium alloy 5182 and Cu–0·15 wt-%Zr electrodes were used in the present numerical work. The strongly temperature dependent electrical, thermal, and mechanical property parameters of the electrodes and aluminium alloy 5182 were taken from Ref. 17. Details of the sheet thickness, electrode diameters, and process parameters used in finite element analysis were the same as those used in experimental simulations, as presented in the previous subsection. Six cases were numerically studied, with the diameter of the pre-drilled hole varying from 0 (new electrode) to 5·0 mm with a constant increment of 1·0 mm.

Results of finite element analysis

The mechanical, electrical, and thermal physical information were all computed and analysed via the finite element method. Many aspects were revealed and quantitatively characterised that could not be measured or obtained by even the most ambitious experimental work, such as the contact area at the sheet/sheet interface, current density level and distribution, temperature

profiles in the workpieces, etc. Details are presented below.

Contact area at interfaces

The contact areas at the electrode/sheet and sheet/sheet interfaces from finite element analysis are shown in Fig. 5 for the electrode force of 5·0 kN.

It can be seen that the nominal contact area (the area contained by the outer diameter of the contact region) between the electrode and the sheet increased gradually with increasing pitting hole diameter. Because the central part of the electrode was hollow, that part did not bear load. When the size of the pitting hole increased, the parts further away from the electrode centreline were pushed into contact to counteract the same electrode force. With increasing pitting hole diameter, the actual contact area (nominal contact area minus the area of no contact in the central region) at the electrode/sheet interface remained fairly constant as the hole diameter varied and was almost the same for all cases. This implied that as the hole diameter increased, more electrode tip surface (having a curved profile) sank into contact with the sheet until the equivalent actual contact area was reached to resist the same electrode force.

The contact areas at the sheet/sheet interface were much larger than that at the electrode/sheet interface for all cases. Increasing the pitting hole diameter D from 0 to 1·0 mm hardly influenced the contact area at the sheet/sheet interface; however, when the pitting hole diameters were increased beyond 3·0 mm, the contact areas at the sheet/sheet interface increased significantly. As had been observed, the nominal contact areas at the electrode/sheet interface were increased with increasing pitting hole diameter; consequently, more material at the sheet/sheet interface was also pushed into contact under the action of the electrode force, and the contact area at the sheet/sheet interface was increased.
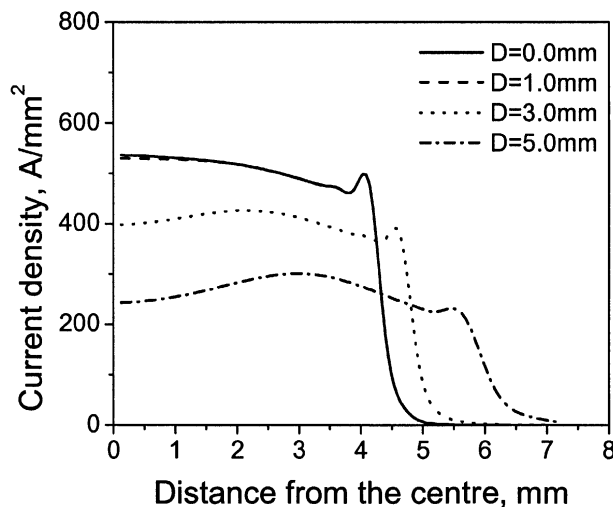
Distribution of current density

The distribution of welding current density at the electrode/sheet interface at the start of welding is shown in Fig. 6. It can be seen that for electrodes without pitting ($D=0$ mm), the current density in the central
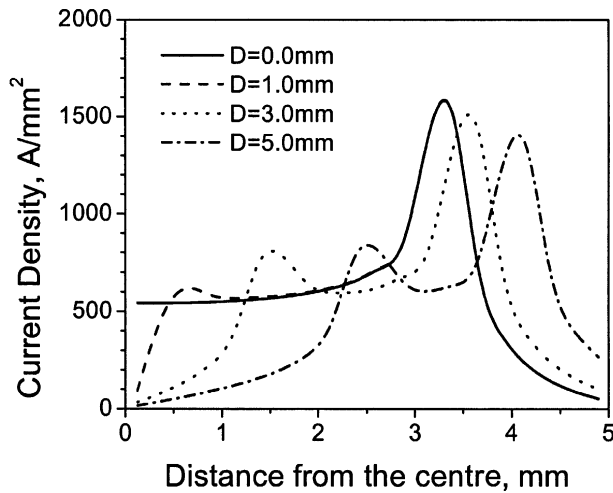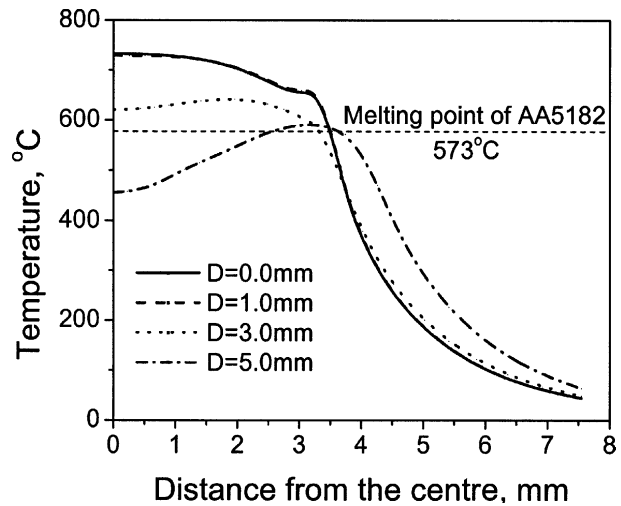
6 Current density distribution at electrode/sheet interface at start of welding for electrodes with various diameters of pre-drilled hole

8 Temperature distribution at sheet/sheet interface at end of welding for electrodes with various pre-drilled hole diameters

region was distributed evenly, and there was a current density peak at the edge of the contact region. As has been explained previously,[15] the current density peak was caused by the 'edge effect', in which the electric current tended to flow into the periphery of the contact region because of the smaller area of the contact region compared with the area of the electrode cross-section. For electrodes with pitting holes, the current density peaks appeared at both the inner and outer edges of the contact ring, and the peak current at the inner edge was lower than that at the outer edge. On increasing the pitting hole diameter, the current density peak value at the outer edge decreased somewhat whereas that at the inner edge increased slightly. Nevertheless, the overall levels of current density did not change significantly for different electrodes because the contact area between the electrode and sheet stayed fairly constant when the diameter of the pitting hole varied, as shown in Fig. 5.

Figure 7 shows the current density distribution at the sheet/sheet interface at the start of spot welding. It can be seen that for the electrode without pitting, the current density was greatest at the centre of the contact region.

There was also a small current density peak at the periphery of the contact region, but the peak current density was lower than that at the centre, and the concentration was not as significant as that at the electrode/sheet interface. Increasing the pitting hole diameter to 1 mm would not exert a strong influence on the current density distribution. However, on increasing the hole diameter to 3·0 mm, the current density at the faying surface reduced greatly owing to the increase in contact area, and the maximum current density no longer occurred at the centreline but started to shift away from the centreline. Increasing the pitting hole diameter further caused the current density to decrease further also, because of the significant increase of contact area at the faying surface, as can be seen from the current density distribution when $D=5·0$ mm. It is well known that the current density is the most important quantity influencing nugget formation and growth because the heat generation is proportional to the square of the welding current. It is predictable that when the electrode pitting developed to a certain degree, and current density was reduced excessively, the heat generated would not be sufficient for nugget formation and growth and only partial melting or even no melting could occur at the faying surface; this has been clearly demonstrated in Fig. 8.

Temperature distribution at end of welding

Temperature distribution at the sheet/sheet interface at the end of spot welding (5 cycles) is shown in Fig. 8. It can be seen that for a new electrode without pitting, the temperature was highest in the central region. The radius of the region at a temperature above 573°C (the melting point of AA5182) was about 3·5 mm, indicating that the diameter of the molten nugget was about 7·0 mm, which was consistent with the experimental observation.[3] Increasing the pitting hole diameter from zero to 1 mm would not affect the dimensions of the melted region, and basically the same size of nugget as that for $D=0$ mm would form under such conditions, as can be concluded from the essentially identical temperature distributions for these two cases ($D=0$ and 1·0 mm). When the pitting hole diameter increased to 3·0 mm, the temperature at the sheet/sheet interface was

7 Current density distribution at sheet/sheet interface at start of welding for electrodes with various pre-drilled hole diameters
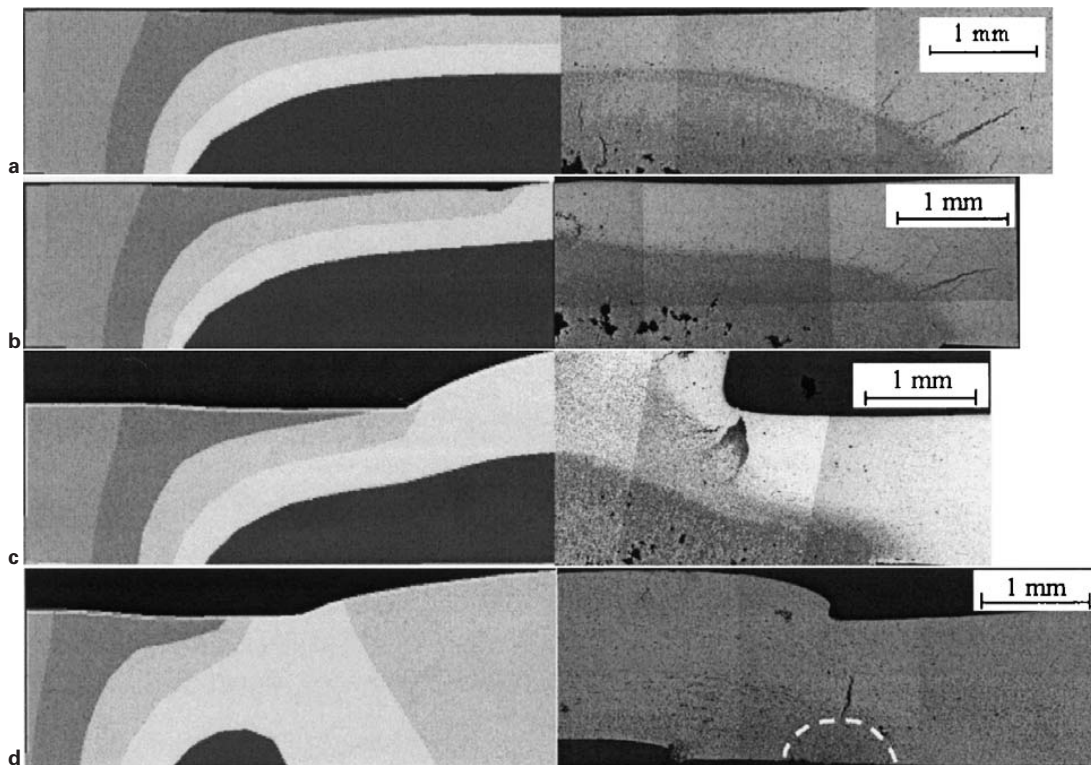
9 Nugget shape and dimensions obtained from numerical prediction (left hand side) and experimental observation (right hand side) for electrodes with pitting hole diameters of *a* 0, *b* 1·0, *c* 3·0, and *d* 5·0 mm

decreased, and the region at a temperature higher than the melting point of the aluminium alloy was reduced, indicating that the thickness and the diameter of the nugget would decrease. For the pitting hole diameter of 5·0 mm, the temperature at the centre part did not reach the melting point of AA5182, indicating that no melting occurred and no nugget formed at the centre; at the same time, it can be seen that a small region about 3 mm away from the centreline reached temperatures above the melting point of the present aluminium alloy, indicating that a nugget in the shape of a ring was formed in that region under such welding conditions.

Comparison between experimental simulations and numerical analysis

Figure 9 shows a direct comparison of the predicted temperature distribution (left hand side of the figure) and the experimentally obtained shape and dimensions of nuggets (right hand side of the figure) on the cross-sections of the samples for $D=0$, 1·0, 3·0, and 5·0 mm, respectively. The dark regions in the finite element analysis results represent the nuggets, which reached temperatures higher than the melting point of AA5182 (573°C). When spot welded with a new electrode, the experimentally obtained nugget diameter was about 7·0 mm (Fig. 9*a*), which agreed very well with the calculation. When the pitting hole was 1·0 mm in diameter, the nugget diameter was almost the same as that for the electrode without pitting (Fig. 9*b*); hence, the presence of small pre-drilled holes in the electrodes did not have a detrimental influence on nugget formation. However, when the pitting hole diameter increased to 3·0 mm, both temperature profile and nugget diameter were reduced significantly (Fig. 9*c*). When the pitting hole diameter reached 5·0 mm, only a small

nugget formed in a toroidal shape without any melting in the central region (Fig. 9*d*). This indicates that severe electrode pitting is unfavourable to the weld quality since a larger pitted area on the electrode surface will result in a larger contact area and lower current density at the sheet/sheet interface, and hence the formation of undersized nuggets. The experimental results are in good agreement with numerical predictions, which proves the validity of the established finite element model in studying the influence of electrode pitting on the spot welding quality.

Summary

The effect of electrode pitting on the weld nugget formation in RSW of an aluminium alloy was investigated using the finite element method. The calculations were validated by a corresponding experimental simulation, in which electrodes (of tip face diameter 10 mm and radius of curvature 50 mm) with a pre-drilled hole of varying diameter were used in RSW of 1·5 mm thickness sheet aluminium alloy 5182 using a medium frequency direct current welder. The results showed that when the pitting hole was small, the temperature, and hence nugget formation, was not affected very strongly. On increasing the pitting hole diameter further, beyond 3·0 mm, the nominal contact area at the electrode/sheet interface increased, whereas the actual contact area at this interface did not change significantly; conversely, the contact area at the sheet/sheet interface was increased significantly on increasing the pitting hole diameter to greater than 3·0 mm, and the current density at this interface was reduced greatly. The temperature and nugget size started to decrease for pitting holes greater than 3·0 mm in diameter. When the pitting hole diameter reached 5·0 mm, a small nugget formed in a

toroidal shape without melting in the central region. The numerical calculation of the nugget shape and dimensions agreed well with the experimental results. The present study confirmed that a severely pitted area on the electrode surface was a major cause of decreased weld quality in terms of nugget size and hence joint strength during RSW of aluminium alloys because of the increased contact area, and hence reduced current density, at the sheet/sheet interface.

Acknowledgement

References

1. B. Irving: *Weld. J.*, 1995, **74**, (8), 29–34.
2. R. M. Rivett and S. A. Westgate: *Met. Constr.*, 1980, **12**, (10), 510–517.
3. S. Fukumoto, I. Lum, E. Biro, D. R. Boomer and Y. Zhou: *Weld. J.*, 2003, **82**, (11), 307s–312s.
4. M. R. Finlay: *Aust. Weld. Res.*, *CRC*, 1996, **18**, 21.
5. G. L. Leone and B. Altshuller: 'Improvement on the resistance spot weldability of aluminum body sheet', Technical Paper 840292, Society of Automotive Engineers, Warrendale, PA, USA, 1984.
6. R. M. Rivett: 'Spot welding electrode life tests on aluminium sheet – effect of parent metal composition and surface treatment', Report 132, The Welding Institute, Abington, Cambs., UK, 1980.
7. E. P. Patrick and D. J. Spinella: Proc. AWS Sheet Metal Welding Conf., Detroit Section VII, Troy, MI, October 1996, American Welding Society, paper B4.
8. Y. Tanaka and M. Noguchi: *Weld. Int.*, 1987, **11**, 1074–1078.
9. M. A. Glagola and A. R. Calvin: 'Nickel plated electrodes for spot welding aluminum', Technical Paper 760167, Society of Automotive Engineers, Warrendale, PA, USA, 1976.
10. R. Ikeda, K. Yasuda, K. Hashiguchi, T. Okita and T. Yahaba: Proc. Advanced Technologies and Processes (IBEC '95), SAE, 44–51; 1995, Michigan, Warren.
11. W. Chuko and J. Gould: Proc. TMS 2001 Annual Meeting, Aluminum Automotive and Joining Symposia, 139–154; 2001, Warrendale, PA, TMS.
12. U. Dilthey and H. Sven: *Weld. Cutting*, 1998, (1), 34–40.
13. I. Lum, S. Fukumoto, E. Biro, D. R. Boomer and Y. Zhou: *Metall. Mater. Trans. A*, 2004, **35A**, (1), 217–226.
14. E. P. Patrick, J. R. Auhl and T. S. Sun: 'Understanding the process mechanisms is key to reliable resistance spot welding aluminum auto body components', Technical Paper 840291, Society of Automotive Engineers, Warrendale, PA, USA, 1984.
15. B. H. Chang, M. V. Li and Y. Zhou: *Sci. Technol. Weld. Joining*, 2001, **6**, (5), 273–280.
16. D. J. Browne, H. W. Chandler, J. T. Evans and J. Wen: *Weld. J.*, 1995, **74**, (10), 339s–344s.
17. 'Metals handbook', 9th edn, Vol. 2, 'Properties and selection: nonferrous alloys and pure metals', 45–92; 1979, Metals Park, OH, USA, American Society for Metals.